PHOTONICS

Direct imaging of isofrequency contours in photonic structures

Emma C. Regan,[1,2]* Yuichi Igarashi,[1,3]* Bo Zhen,[1,4]*† Ido Kaminer,[1] Chia Wei Hsu,[5] Yichen Shen,[1] John D. Joannopoulos,[1] Marin Soljačić[1]

The isofrequency contours of a photonic crystal are important for predicting and understanding exotic optical phenomena that are not apparent from high-symmetry band structure visualizations. We demonstrate a method to directly visualize the isofrequency contours of high-quality photonic crystal slabs that show quantitatively good agreement with numerical results throughout the visible spectrum. Our technique relies on resonance-enhanced photon scattering from generic fabrication disorder and surface roughness, so it can be applied to general photonic and plasmonic crystals or even quasi-crystals. We also present an analytical model of the scattering process, which explains the observation of isofrequency contours in our technique. Furthermore, the isofrequency contours provide information about the characteristics of the disorder and therefore serve as a feedback tool to improve fabrication processes.

INTRODUCTION

Although band structures are useful for understanding and predicting the optical properties of photonic crystal (PhC) slabs, they are typically calculated or measured only along high-symmetry directions because of computation and time constraints. A more comprehensive understanding of a PhC slab lies in its isofrequency contours: slices in two-dimensional (2D) momentum space (k_x, k_y) of constant frequency ω. In particular, isofrequency contours are essential for understanding phenomena that depend on the direction of group velocities, such as negative refraction (*1*), supercollimation (*2*, *3*), and superlensing (*4*). In recent years, the full dispersion of radiative PhC slab resonances has gained further interest for their important roles in topics including non-Hermitian physics (*5*–*7*), bound states in the continuum (*8*, *9*), zero-index metamaterials (*10*, *11*), lasers (*12*), sensors (*13*), coherent perfect absorbers (*14*, *15*), solar cells (*16*), radiative cooling (*17*, *18*), and structural color (*19*). However, obtaining isofrequency contours is not trivial, and current experimental techniques involve samples with strong disorder (*20*), additional fabrication steps (*21*, *22*), or sophisticated experimental setups (*23*). Fourier plane microscopy is another widely used method (*24*–*28*) and can provide isofrequency contours inside or outside the light cone, yet the use of mode-coupled fluorescence directly limits the accessible wavelength range. These methods have been applied to photonic resonances in dielectric structures (*20*, *21*, *23*), as well as to plasmonic resonances in metallic structures (*22*, *24*–*31*).

As an alternative, we demonstrate direct imaging of isofrequency contours using resonance-enhanced photon scattering arising from minimal, intrinsic fabrication disorder in a "pristine" sample. The experimental isofrequency contours show good quantitative agreement with numerical results throughout the visible wavelength regime. To understand the underlying physical process, we use temporal coupled-mode theory (TCMT) (*32*–*34*) to show that scattering is enhanced for on-resonance photons and that the angular distribution of scattered photons recreates the isofrequency contours in the far field. Intrinsic disorder (*35*) and resonance-enhanced scattering (*36*–*38*) have been used to study localized photonic modes, but we show that this scattering process can also be used to probe large-area, delocalized resonances and their corresponding isofrequency contours.

Additionally, our results reflect information about the characteristic fabrication disorder in a PhC slab and thus serve as a feedback method for improving the fabrication processes. This technique may also be extended to quasi-crystals and may provide an experimental route to obtain their isofrequency contours, which are quite challenging to obtain using current numerical tools.

RESULTS

Direct imaging of isofrequency contours

The direct imaging mechanism relies on a simple process (Fig. 1A). We excite a PhC slab resonance using incident light at the proper frequency ω and in-plane wavevector (k_x, k_y). The natural disorder in the sample scatters light in this resonance to resonances at other wavevectors, depending on the spatial Fourier coefficients of the fabrication disorder. These resonances then radiate photons, which recreate the isofrequency contour in the far field. By scanning the frequency of the light source and tuning the incident angle accordingly, we can visualize isofrequency contours throughout the visible spectrum. A quantitative description of the resonance-enhanced scattering process is presented in the next section.

To demonstrate this technique, we fabricated a hole-array PhC slab and observed the distribution of scattered photons. A large-area PhC slab was fabricated using interference lithography (*39*). As shown in Fig. 1B, a high-quality square lattice of cylindrical air holes with a radius of 103 nm and a periodicity of 336 nm was patterned into a Si_3N_4 slab with a thickness of 180 nm on top of a SiO_2 substrate. The sample was then mounted in a cell filled with liquid of refractive index n_{liquid} = 1.46, which was then placed on a rotation stage (Newport) for precise control over the incident angle (Fig. 1C). Because we use liquid with the same refractive index as the SiO_2 substrate, our sample has an up-down mirror symmetry, and thus, we can separate the resonances into transverse magnetic–like (TM-like; odd-in-*z*) and transverse electric–like (TE-like; even-in-*z*) modes. The sample was then excited with a broadband supercontinuum source (SuperK, NKT) through a narrow (10 nm) band-pass filter, as shown in Fig. 1C, or with a narrow-linewidth laser. A polarizer was placed along the beam path to allow selection between

[1]Research Laboratory of Electronics, Massachusetts Institute of Technology, Cambridge, MA 02139, USA. [2]Department of Physics, Wellesley College, Wellesley, MA 02481, USA. [3]Smart Energy Research Laboratories, NEC Corporation, 34 Miyuiga-ka, Tsukuba, Ibaraki 305-8501, Japan. [4]Physics Department and Solid State Institute, Technion, Haifa 32000, Israel. [5]Department of Applied Physics, Yale University, New Haven, CT 06520, USA.
*These authors contributed equally to this work.
†Corresponding author. Email: bozhen@mit.edu

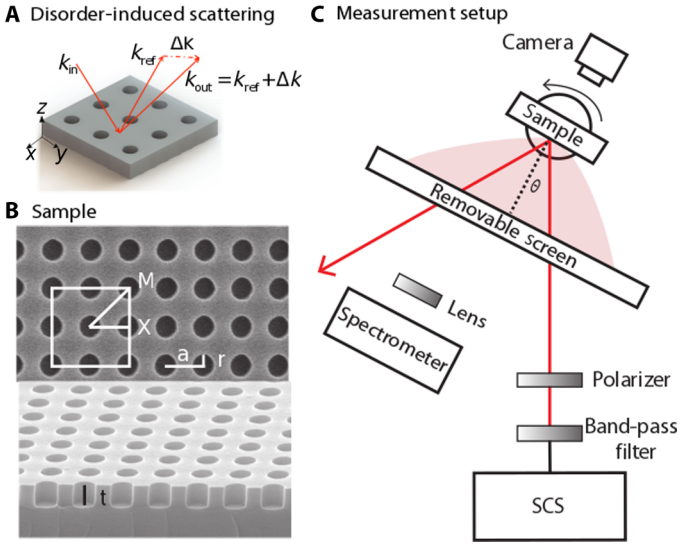

Fig. 1. Resonance-enhanced scattering concept and experimental setup. (**A**) Scattering of light with incident in-plane wavevector k_{in} to wavevector $k_{out} = k_{ref} + \Delta k$ due to weak, intrinsic disorder in the sample. (**B**) Scanning electron microscopy images of the near-pristine PhC samples with a = 336 nm, r = 103 nm, and t =180 nm: top view (top panel) and side view (bottom panel). (**C**) Schematic drawing of the experimental setup. The removable screen has slits for the incident and the specularly reflected beams, but it blocks scattered light, showing the projected isofrequency contours. For a later experiment, the screen and band-pass filter are removed, so broadband scattered light can couple into the spectrometer for enhanced scattering measurements. Supercontinuum source (SCS) and band-pass filter could be replaced with a laser.

s- and p-polarization. For this experiment, we chose an s-polarized source and the incident angle to excite the TM-like resonances. We placed a removable paper screen in front of the sample, with a slit for the incident and mirror-reflected beams to pass through. For each wavelength, we used a camera (DDC1645C, Thorlabs) to take an image of the screen that clearly shows the angular distribution of the scattered photons. Examples of photon distribution are shown in Fig. 2, with excitation wavelengths centered at 488, 514, 532, 550, 580, 600, 610, and 620 nm. Contours for 488 and 514 nm were created with an argon laser (Stellar-Pro, Modu-Laser), and the others were created using the supercontinuum source with band-pass filters.

We also computed isofrequency contours for the same frequencies by simulating the band structure $\omega(k_x, k_y)$ using MEEP (*40*), a freely available finite-difference time-domain software package, and COMSOL, a finite-element analysis software package. MEEP and COMSOL were used for different frequency ranges to avoid simulation artifacts, which are common when simulating a wide range of angles and frequencies. Our experimental results (Fig. 2, bottom panels) show quantitative agreement with the numerical isofrequency contours for the same wavelengths (Fig. 2, top panels), with a small, systematic difference in the angle present in the experimental setup that can be avoided with a careful angle calibration, as well as a more precise knowledge of the geometric parameters of the PhC slab.

Resonance-enhanced scattering

To better understand the imaging technique, we present a theoretical treatment of the resonance-enhanced scattering process. It is well known that macroscopic optical resonances can be used to trap light and therefore enhance nonradiative processes, like optical absorption. This leads to intriguing physical phenomena, such as coherent perfect absorption (*41*, *42*), critically coupled resonators (*43*), and complete photon absorption in a graphene monolayer (*11*). However, the possibility of using large-area resonances to enhance scattering remains largely unstudied. In this section, we consider a general PhC slab and compute the enhancement of scattered light from intrinsic fabrication disorder and surface roughness under both on- and off-resonance conditions.

An effective tool to understand this process is TCMT (*32*–*34*). Consider a collimated beam incident on the PhC slab that excites a resonance. We treat the Rayleigh scattering from the disorder of the slab as a nonradiative decay channel for the resonance, because photons being scattered do not contribute to the power in the transmission and reflection channels, similar to photons being nonradiatively absorbed. For high-quality PhC slabs made of low-loss dielectrics, the decay channel for the resonances via material absorption is negligible (*39*, *44*) compared to scattering. When the scattering is weak and the lifetime of the resonance is sufficiently long, we can approximate the total amount of scattered light as (*32*)

$$\frac{P_{scat}}{P_{in}} = \frac{2\gamma_r\gamma_{scat}}{(\omega-\omega_0)^2+(\gamma_r+\gamma_{scat})^2} \quad (1)$$

where P_{scat} is the scattered power, P_{in} is the incident power, ω is the incoming photon frequency, ω_0 is the resonance frequency, γ_r is the radiative decay rate of the resonance, and γ_{scat} is the decay rate due to scattering from disorder (section S1). Here, we consider only one resonance in the PhC slab, but the generalization into multiple resonances is straightforward. From Eq. 1, the scattering rate is most efficient (P_{scat}/P_{in} = 50%) when the system is driven on resonance ($\omega = \omega_0$) and the radiative decay rate equals the scattering decay rate ($\gamma_r = \gamma_{scat}$). This result agrees with the well-known results in critical coupling for absorption enhancement (*11*, *43*, *45*). By engineering the quality of the resonances in a PhC, this technique can accommodate samples with different levels of disorder.

Next, we consider the angular distribution of the scattered photons, which leads to the formation of isofrequency contours in the far field. The resonance-enhanced scattering can be modeled as a three-step process (Fig. 1A). In the first step, incoming light with frequency ω excites a resonance at in-plane wavevector k_{in}. In the second step, disorder couples the resonance at k_{in} to resonances at other wavevectors, $k_{out} = k_{ref} + \Delta k$. The strength of this coupling depends on the spatial Fourier coefficient of the disorder at Δk, $|F_{\Delta k}|^2$. In the third step, resonances at k_{out} radiate photons into the far field with outgoing angles specified by frequency ω and in-plane momentum k_{out}. The photons acquire random phases through the disorder coupling (second step), so their subsequent reradiation (third step) can be modeled as the radiation from a collection of randomly polarized dipoles with number density of N_0 and dipole strength of μ. As a result, the decay rate into the radiation channel with in-plane wavevector k_{out} and frequency ω depends on the spectral density of states (*46*) in the vicinity of the PhC slabs and can therefore be approximated as

$$\Gamma(k_{out},\omega) = \frac{N_0\pi\omega|\mu|^2}{3\hbar\epsilon}\sum_n \alpha_n \frac{1}{\pi}\frac{\Delta\omega^n_{k_{out}}}{(\omega-\omega^n_{k_{out}})^2+(\Delta\omega^n_{k_{out}})^2} \quad (2)$$

Here, μ is the average electric dipole strength depending on the total power in the scattered photons, n labels different PhC resonances at a

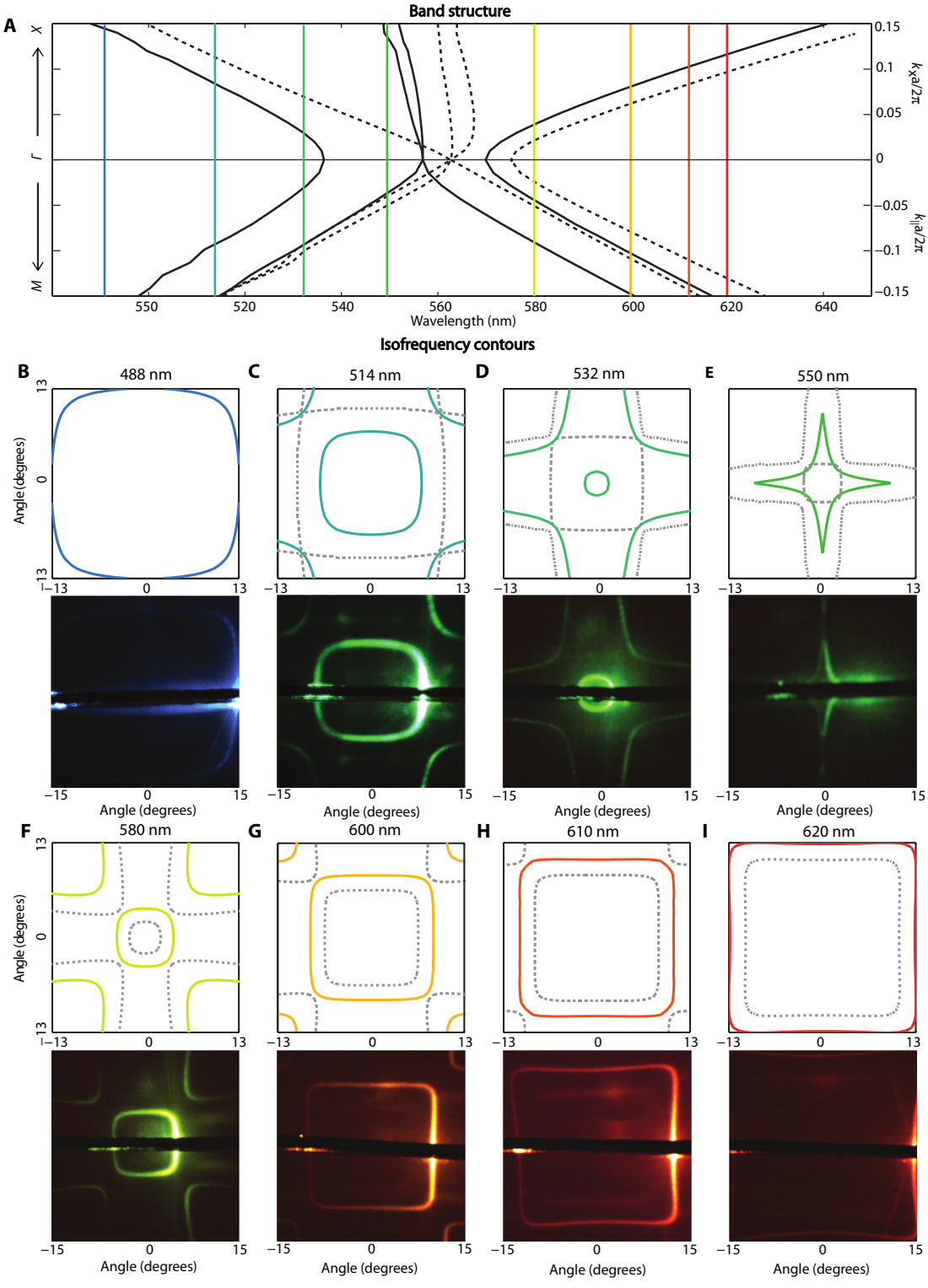

Fig. 2. Direct visualization of isofrequency contours. (**A**) Numerical simulation (COMSOL) of band structure, with the colored vertical lines corresponding to wavelengths of the isofrequency contours below. TE-like bands are dashed and TM-like bands are solid. Numerical [MEEP for (**B**) to (**E**); COMSOL for (**F**) to (**I**)] and experimental isofrequency contours at (B) 488 nm, (C) 514 nm, (D) 532 nm, (E) 550 nm, (F) 580 nm, (G) 600 nm, (H) 610 nm, and (I) 620 nm. Note that the numerical and experimental contours are shown with different scales due to small, systematic differences in angles that can be avoided with a careful angle calibration and knowledge of the precise geometric parameters of the sample. TE-like contours are dashed and TM-like contours are solid. In all cases, the incident beam excited a TM-like resonance. The experimental data use incident light with s-polarization at angles of (B) −14.4°, (C) −8.0°, (D) −2.6°, (E) −5.6°, (F) −5.1°, (G) −9.8°, (H) −12.4°, and (I) −15.4°. The dark, horizontal line in the middle of the experimental contours is the slit in the screen for the incident and the specularly reflected beams to pass through.

given k_{out}, α_n represents the coupling between the initially excited resonance and the final resonance mediated by the surface roughness, $\Delta\omega^n_{k_{out}}$ are the linewidths of the outgoing resonances accounting for both radiative and nonradiative decay, and $\omega^n_{k_{out}}$ are the central frequencies of the outgoing resonances (section S2). From Eq. 2, it is clear that scattering is maximized when the emission frequency is on-resonance with one of the resonance frequencies for a given momentum ($\omega = \omega^n_{k_{out}}$). Therefore, for incident light with frequency ω_0, we expect large scattering for the momenta k_{out} that provide resonances also at ω_0. Accordingly, the highest-intensity positions in the far field will correspond to the isofrequency contours of this PhC at the frequency of ω_0.

To experimentally demonstrate that this technique relies on resonance-enhanced scattering, we measured the spectrum of the scattered photons from the PhC slab when excited with a supercontinuum source. We removed the paper screen in the experimental setup shown in Fig. 1C. Scattered photons were then collected using a lens with a numerical aperture (NA) of 0.25 and a focal length of 5 cm that was placed in front of a spectrometer with a spectral resolution of 0.03 nm (HR4000, Ocean Optics). The distance between the spectrometer and the lens was optimized to maximize the coupling of the scattered photons into the spectrometer. The positions of the spectrometer and the lens were fixed during the experiment, and the sample was rotated between 0° and 8° from the normal direction with a step size of 0.1°. Throughout this measurement, we ensured that the directly reflected beam was not captured by the lens, so only scattered light was recorded. We note that the two scattering measurements presented (Figs. 2 and 3) characterize different physical properties. For Fig. 2, the excitation source is a laser (or a narrow-band source) with a well-defined wavelength. Characterization of the angular distribution of the scattered photons leads to the isofrequency contours. On the other hand, for Fig. 3, the excitation source is a broadband supercontinuum. For detection, we do not distinguish between outgoing angles (by placing a lens with NA = 0.25 in front of the spectrometer) but instead only measure the spectrum of all scattered photons.

The experimental scattering spectra are shown in the middle column of Fig. 3. The scattering peaks show good quantitative agreement with the numerical results for the locations of the resonances obtained from COMSOL (shown in the left column). This can be understood from Eq. 1: the enhancement is maximized when the incident light frequency is on resonance. S- and p-polarized light excite different resonances due to symmetry: the incident beam and the structure are both mirror-symmetric in the y direction. Therefore, the even (odd) incident beam can only excite even (odd) resonances with respect to y, as described by Hsu *et al.* (*8*) and Lee *et al.* (*44*). Exemplary line cuts of the scattering spectra at 4.3° are shown in the right column, which show that the experimental results agree well with the expected Lorentzian line shapes.

As we can see in Fig. 3, the resonance-enhanced scattering process is also an efficient way to measure PhC band structures, avoiding the shortcomings of other standard techniques. For example, reflection measurements are often used to measure band structures because Fano features in the spectrum indicate resonances (*47*). However, reflection measurements require constantly moving the spectrometer to maintain overlap with the specularly reflected beam. On the other hand, enhanced fluorescence measurements require additional incorporation of emitters and are limited by their emission bandwidth (*48*). Finally, enhanced absorption measurements inevitably lower the quality factors of the resonances because of the incorporation of a lossy medium (*49*). The method that we present takes advantage of minimal, generic fabrication errors and surface roughness in any high-quality resonator (for example, the resonances we measured have quality factors as high as $Q \approx 5000$), does not require moving the spectrometer, and allows for a fast and direct measurement of the resonance central frequencies and the quality factors.

DISCUSSION

The experimental isofrequency contours also give information about the characteristic fabrication errors in the PhC slab, which is not possible to obtain otherwise. As shown in Fig. 2, for a given frequency, the contours corresponding to TM-like resonances (solid lines) are significantly brighter than those corresponding to the TE-like resonances (dashed lines). This means that the disorder in our sample predominantly couples the initial incoming TM-like resonance to outgoing TM-like resonances (instead of TE-like resonances), which suggests that the major sources of fabrication errors also satisfy up-down mirror symmetry. Therefore, we know that the fabrication errors that do not break up-down mirror symmetry (for example, distortions of the hole shape in the interference process) dominate over those errors that break the up-down mirror symmetry (for example, oblique side walls in the etching process). Furthermore, we can determine the characteristic length scale of the disorder by analyzing the intensity of the isofrequency contours (section S3).

Additionally, resonance-enhanced scattering has applications in several display technologies. In particular, transparent displays have been realized using plasmonic resonances (*50*, *51*), but the high-quality factors of photonic resonances, due to negligible absorption and narrow linewidths, may allow for significantly better performance. If the isofrequency contour is engineered to be at large angles and therefore

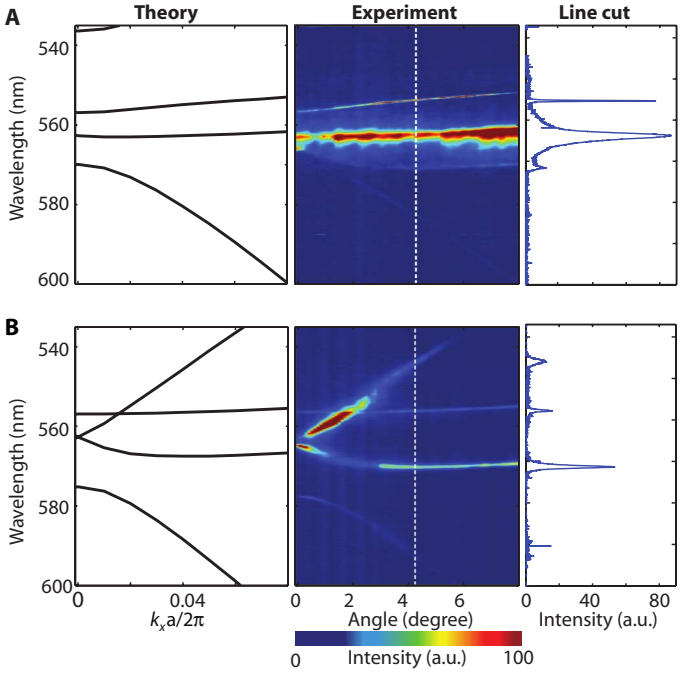

Fig. 3. Experimental verification of resonance-enhanced scattering. Numerically calculated band structure (left) and experimentally measured scattering spectrum (middle) for (**A**) s-polarized and (**B**) p-polarized light. The right column shows line cuts at 4.3° from the experimental scattering spectrum.

far away from a viewing audience, the resonance-enhanced scattering process can be used for a transparent display. A large portion of the ambient light will pass through the display, but light from a laser projector incident at resonant angles will be scattered and will form an image. Projecting incoming light of different polarization states or wavelengths could allow for a transparent 3D display. Furthermore, engineering isofrequency contours to direct photons to different angles could create a privacy screen (*52*). By projecting light at a specified incident angle, viewers at particular directions could see the strongly scattered light, whereas viewers at other angles can only see a transparent panel.

In conclusion, this article presents theoretical and experimental results on enhanced photon scattering in the presence of a large-area, nearly pristine PhC slab. We use this phenomenon to measure the band structure of a PhC slab and to directly reconstruct its isofrequency contours. The isofrequency contours also give information about the dominant fabrication errors in a sample and can thus be a useful tool for improving the fabrication process.

MATERIALS AND METHODS

Sample fabrication

The Si_3N_4 layer was grown by low-pressure chemical vapor deposition on a 6-μm-thick cladding of SiO_2 on the backbone of a silicon wafer (LioniX). The wafer was then coated with an anti-reflection polymer coating, a thin SiO_2 intermediate layer, and a layer of negative photoresist. The square lattice pattern was created with Mach-Zehnder interference lithography using a 325-nm He/Cd laser. The angle between the two arms of the laser beam was chosen for a periodicity of 336 nm, and the hole exposure was selected for a hole radius of 103 nm. After exposures, the pattern in the photoresist was transferred to the Si_3N_4 by reactive-ion etching.

SUPPLEMENTARY MATERIALS

Supplementary material for this article is available at http://advances.sciencemag.org/cgi/content/full/2/11/e1601591/DC1

section S1. Derivation of total scattered light.
section S2. Derivation of resonance decay rate.
section S3. Disorder characterization.
fig. S1. Schematic of the TCMT setup showing resonator, channels, and decay lifetimes.
fig. S2. Characterization of spatial Fourier coefficients of disorder using computed mode overlap and experimental isofrequency contours.
References (*53*, *54*)

REFERENCES AND NOTES

1. C. Luo, S. G. Johnson, J. D. Joannopoulos, J. B. Pendry, All-angle negative refraction without negative effective index. *Phys. Rev. B* **65**, 201104 (2002).
2. H. Kosaka, T. Kawashima, A. Tomita, M. Notomi, T. Tamamura, T. Sato, S. Kawakami, Self-collimating phenomena in photonic crystals. *Appl. Phys. Lett.* **74**, 1212–1214 (1999).
3. P. T. Rakich, M. S. Dahlem, S. Tandon, M. Ibanescu, M. Soljaćič, G. S. Petrich, J. D. Joannopoulos, L. A. Kolodziejski, E. P. Ippen, Achieving centimeter-scale supercollimation in a large-area two-dimensional photonic crystal. *Nat. Mater.* **5**, 93–96 (2006).
4. H. Kosaka, T. Kawashima, A. Tomita, M. Notomi, T. Tamamura, T. Sato, S. Kawakami, Superprism phenomena in photonic crystals. *Phys. Rev. B* **58**, R10096–R10099 (1998).
5. B. Zhen, C. W. Hsu, Y. Igarashi, L. Lu, I. Kaminer, A. Pick, S.-L. Chua, J. D. Joannopoulos, M. Soljačić, Spawning rings of exceptional points out of Dirac cones. *Nature* **525**, 354–358 (2015).
6. Z. Lin, A. Pick, M. Lončar, A. W. Rodriguez, Enhanced spontaneous emission at third-order Dirac exceptional points in inverse-designed photonic crystals. *Phys. Rev. Lett.* **117**, 107402 (2016).
7. A. Cerjan, A. Raman, S. Fan, Exceptional contours and band structure design in parity-time symmetric photonic crystals. *Phys. Rev. Lett.* **116**, 203902 (2016).
8. C. W. Hsu, B. Zhen, J. Lee, S.-L. Chua, S. G. Johnson, J. D. Joannopoulos, M. Soljačić, Observation of trapped light within the radiation continuum. *Nature* **499**, 188–191 (2013).
9. C. W. Hsu, B. Zhen, A. D. Stone, J. D. Joannopoulos, M. Soljačić, Bound states in the continuum. *Nat. Rev. Mater.* **1**, 16048 (2016).
10. X. Huang, Y. Lai, Z. H. Hang, H. Zheng, C. T. Chan, Dirac cones induced by accidental degeneracy in photonic crystals and zero-refractive-index materials. *Nat. Mater.* **10**, 582–586 (2011).
11. Y. Li, S. Kita, P. Muñoz, O. Reshef, D. I. Vulis, M. Yin, M. Lončar, E. Mazur, On-chip zero-index metamaterials. *Nat. Photon.* **9**, 738–742 (2016).
12. K. Hirose, Y. Liang, Y. Kurosaka, A. Watanabe, T. Sugiyama, S. Noda, Watt-class high-power, high-beam-quality photonic-crystal lasers. *Nat. Photon.* **8**, 406–411 (2014).
13. A. A. Yanik, A. E. Cetin, M. Huang, A. Artar, S. H. Mousavi, A. Khanikaev, H. Altug, Seeing protein monolayers with naked eye through plasmonic Fano resonances**.** *Proc. Natl. Acad. Sci. U.S.A.* **108**, 11784–11789 (2011).
14. J. R. Piper, S. Fan, Total absorption in a graphene monolayer in the optical regime by critical coupling with a photonic crystal guided resonance. *ACS Photon.* **1**, 347–353 (2014).
15. H. Zhou, B. Zhen, C. W. Hsu, O. D. Miller, S. G. Johnson, J. D. Joannopoulos, M. Soljačić, Perfect single-sided radiation and absorption without mirrors. *Optica* **3**, 1079–1086 (2016).
16. Z. Yu, A. Raman, S. Fan, Fundamental limit of nanophotonic light trapping in solar cells. *Proc. Natl. Acad. Sci. U.S.A.* **107**, 17491–17496 (2010).
17. E. Rephaeli, A. Raman, S. Fan, Ultrabroadband photonic structures to achieve high-performance daytime radiative cooling. *Nano Lett.* **13**, 1457–1461 (2013).
18. L. Zhu, A. P. Raman, S. Fan, Radiative cooling of solar absorbers using a visibly transparent photonic crystal thermal blackbody. *Proc. Natl. Acad. Sci. U.S.A.* **112**, 12282–12287 (2015).
19. Y. Shen, V. Rinnerbauer, I. Wang, V. Stelmakh, J. D. Joannopoulos, M. Soljačić, Structural colors from Fano resonances. *ACS Photon.* **2**, 27–32 (2014).
20. L. Shi, H. Yin, X. Zhu, X. Liu, J. Zi, Direct observation of iso-frequency contour of surface modes in defective photonic crystals in real space. *Appl. Phys. Lett.* **97**, 251111 (2010).
21. N. Le Thomas, R. Houdré, D. M. Beggs, T. F. Krauss, Fourier space imaging of light localization at a photonic band-edge located below the light cone. *Phys. Rev. B* **79**, 033305 (2009).
22. A. Giannattasio, W. L. Barnes, Direct observation of surface plasmon-polariton dispersion. *Opt. Express* **13**, 428–434 (2005).
23. R. Sapienza, T. Coenen, J. Renger, M. Kuttge, N. F. van Hulst, A. Polman, Deep-subwavelength imaging of the modal dispersion of light. *Nat. Mater.* **11**, 781–787 (2012).
24. D. Dominguez, N. Alharbi, M. Alhusain, A. A. Bernussi, L. G. de Peralta, Fourier plane imaging microscopy. *J. Appl. Phys.* **116**, 103102 (2014).
25. C. J. Regan, A. Krishnan, R. Lopez-Boada, L. Grave de Peralta, A. A. Bernussi, Direct observation of photonic Fermi surfaces by plasmon tomography. *Appl. Phys. Lett.* **98**, 151113 (2011).
26. C. J. Regan, L. Grave de Peralta, A. A. Bernussi, Directivity and isotropic band-gap in 12-fold symmetry plasmonic quasi-crystals with small index contrast. *Appl. Phys. Lett.* **99**, 181104 (2011).
27. S. P. Frisbie, C. F. Chesnutt, M. E. Holtz, A. Krishnan, L. G. De Peralta, A. A. Bernussi, Image formation in wide-field microscopes based on leakage of surface plasmon-coupled fluorescence. *IEEE Photonics* **1**, 153–162 (2009).
28. D. G. Zhang, X. Yuan, A. Bouhelier, Direct image of surface-plasmon-coupled emission by leakage radiation microscopy. *Appl. Opt.* **49**, 875–879 (2010).
29. S. C. Kitson, W. L. Barnes, G. W. Bradberry, J. R. Sambles, Surface profile dependence of surface plasmon band gaps on metallic gratings. *J. Appl. Phys.* **79**, 7383–7385 (1996).
30. T. J. Constant, A. P. Hibbins, A. J. Lethbridge, J. R. Sambles, E. K. Stone, P. Vukusic, Direct mapping of surface plasmon dispersion using imaging scatterometry. *Appl. Phys. Lett.* **102**, 251107 (2013).
31. T. J. Constant, P. Vukusic, A. P. Hibbins, J. R. Sambles**,** Surface plasmons at the Brillouin zone boundary of an oblique lattice. *Appl. Phys. Lett.* **106**, 091106 (2015).
32. J. D. Joannopoulos, S. G. Johnson, J. N. Winn, R. D. Meade, *Photonic Crystals: Molding the Flow of Light* (Princeton Univ. Press, ed. 2, 2011).
33. S. Fan, W. Suh, J. D. Joannopoulos**,** Temporal coupled-mode theory for the Fano resonance in optical resonators. *J. Opt. Soc. Am. A* **20**, 569–572 (2003).
34. W. Suh, Z. Wang, S. Fan, Temporal coupled-mode theory and the presence of nonorthogonal modes in lossless multimode cavities. *IEEE J. Quant. Electron.* **40**, 1511–1518 (2004).
35. R. Faggini, A. Baron, X. Zang, L. Lalouat, S.A. Schulz, B. O'Regan, K. Vynck, B. Cluzel, F. de Fornel, T. F. Krauss, P. Lalanne, Lower bound for the spatial extent of localized modes in photonic-crystal waveguides with small random imperfections. *Sci. Rep.* **6**, 27037 (2016).

36. M. W. McCutcheon, G. W. Rieger, I. W. Cheung, J. F. Young, D. Dalacu, S. Frédérick, P. J. Poole, G. C. Aers, R. L. Williams, Resonant scattering and second-harmonic spectroscopy of planar photonic crystal microcavities. *Appl. Phys. Lett.* **87**, 221110 (2005).
37. M. Galli, S. L. Portalupi, M. Belotti, L. C. Andreani, L. O'Faolain, T. F. Krauss, Light scattering and Fano resonances in high-*Q* photonic crystal nanocavities. *Appl. Phys. Lett.* **94**, 071101 (2009).
38. S. L. Portalupi, M. Galli, M. Belotti, L. C. Andreani, T. F. Krauss, L. O'Faolain, Deliberate versus intrinsic disorder in photonic crystal nanocavities investigated by resonant light scattering. *Phys. Rev. B* **84**, 045423 (2011).
39. J. Lee, B. Zhen, S.-L. Chua, O. Shapira, M. Soljačić, Fabricating centimeter-scale high quality factor two-dimensional periodic photonic crystal slabs. *Opt. Express* **22**, 3724–3731 (2014).
40. A. F. Oskooi, D. Roundy, M. Ibanescu, P. Bermel, J. D. Joannopoulos, S. G. Johnson, MEEP: A flexible free-software package for electromagnetic simulation by the FDTD method. *Comput. Phys. Commun.* **181**, 687–702 (2010).
41. Y. D. Chong, L. Ge, H. Cao, A. D. Stone, Coherent perfect absorbers: Time-reversed lasers. *Phys. Rev. Lett.* **105**, 053901 (2010).
42. W. Wan, Y. Chong, L. Ge, H. Noh, A. D. Stone, H. Cao, Time-reversed lasing and interferometric control of absorption. *Science* **331**, 889–892 (2011).
43. J. R. Tischler, M. S. Bradley, V. Bulović, Critically coupled resonators in vertical geometry using a planar mirror and a 5 nm thick absorbing film. *Opt. Lett.* **31**, 2045–2047 (2006).
44. J. Lee, B. Zhen, S.-L. Chua, W. Qiu, J. D. Joannopoulos, M. Soljačić, O. Shapira, Observation and differentiation of unique high-*Q* optical resonances near zero wave vector in macroscopic photonic crystal slabs. *Phys. Rev. Lett.* **109**, 067401 (2012).
45. D. L. C. Chan, I. Celanovic, J. D. Joannopoulos, M. Soljačić, Emulating one-dimensional resonant *Q*-matching behavior in a two-dimensional system via Fano resonances. *Phys. Rev. A* **74**, 064901 (2006).
46. R. C. McPhedran, L. C. Botten, J. McOrist, A. A. Asatryan, C. M. de Sterke, N. A. Nicorovici, Density of states functions for photonic crystals. *Phys. Rev. E* **69**, 016609 (2004).
47. S. Fan, J. D. Joannopoulos, Analysis of guided resonances in photonic crystal slabs. *Phys. Rev. B* **65**, 235112 (2002).
48. B. Zhen, S.-L. Chua, J. Lee, A. W. Rodriguez, X. Liang, S. G. Johnson, J. D. Joannopoulos, M Soljačić, O. Shapira, Enabling enhanced emission and low-threshold lasing of organic molecules using special Fano resonances of macroscopic photonic crystals. *Proc. Natl. Acad. Sci. U.S.A.* **110**, 13711–13716 (2013).
49. T. Xu, M. S. Wheeler, H. E. Ruda, M. Mojahedi, J. S. Aitchison, The influence of material absorption on the quality factor of photonic crystal cavities. *Opt. Express* **17**, 8343–8348 (2009).
50. C. W. Hsu, B. Zhen, W. Qiu, O. Shapira, B. G. DeLacy, J. D. Joannopoulos, M. Soljačić, Transparent displays enabled by resonant nanoparticle scattering. *Nat. Commun.* **5,** 3152 (2014).
51. K. Saito, T. Tatsuma, A transparent projection screen based on plasmonic Ag nanocubes. *Nanoscale* **7**, 20365–20368 (2015).
52. Y. Shen, C. W. Hsu, Y. X. Yeng, J. D. Joannopoulos, M. Soljačić**,** Broadband angular selectivity of light at the nanoscale: Progress, applications, and outlook. *Appl. Phys. Rev.* **3**, 011103 (2016).
53. L. Novotny, B. Hecht, *Principles of Nano-Optics* (Cambridge Univ. Press, 2006).
54. M. Boroditsky, R. Vrijen, T. F. Krauss, R. Coccioli, R. Bhat, E. Yablonovitch, Spontaneous emission extraction and Purcell enhancement from thin-film 2-d photonic crystals. *J. Lightwave Technol.* **17**, 2096–2112 (1999).

Acknowledgments: We are grateful to S. Kooi for his help with the experiments. We also thank O. Miller, N. Rivera, Y. Yang, and H. Zhou for helpful discussions. **Funding:** This work was partly supported by the Army Research Office through the Institute for Soldier Nanotechnologies under contract no. W911NF-13-D-0001. The fabrication of the sample was supported by S3TEC, an Energy Frontier Research Center funded by the U.S. Department of Energy under grant no. DE-SC0001299. B.Z. was partially supported by the United States–Israel Binational Science Foundation under award no. 2013508. I.K. was supported in part by Marie Curie grant no. 328853-MC-BSiCS. C.W.H. was partly supported by the NSF through grant no. DMR-1307632. **Author contributions:** B.Z. conceived the idea. E.C.R., Y.I., and B.Z. conducted the experiments, and E.C.R. did the numerical analysis. E.C.R. and B.Z. wrote the manuscript, and all other authors contributed to editing the manuscript. **Competing interests:** The authors declare that they have no competing interests. **Data and materials availability:** All data needed to evaluate the conclusions in the paper are present in the paper and/or the Supplementary Materials. Additional data related to this paper may be requested from the authors.

Submitted 11 July 2016
Accepted 20 October 2016
Published 25 November 2016
10.1126/sciadv.1601591

Citation: E. C. Regan, Y. Igarashi, B. Zhen, I. Kaminer, C. W. Hsu, Y. Shen, J. D. Joannopoulos, M. Soljačić, Direct imaging of isofrequency contours in photonic structures. *Sci. Adv.* **2**, e1601591 (2016).